

Full 3D Antenna Modelling based on Fourier Transformation

Stephan Häfner, Robert Müller, Reiner S. Thomä
 Electronic Measurement Engineering Group
 Technische Universität Ilmenau
 98684 Ilmenau, Germany
 Email: stephan.haefner@tu-ilmenau.de

Abstract—We describe an extension of the known Effective Aperture Distribution Function (EADF) approach to fully model an antenna in terms of azimuth, elevation and frequency. The extension also bases on Fourier transformation of measured or simulated antenna responses and is stated as Effective Time-Aperture Distribution Function (ETADF). We also propose a method to automatically de-noise the sampled antenna responses by estimating the model order. Furthermore, an efficient calculation method for off-grid sampling points is presented.

Keywords – Algebraic Antenna Model, Wavefield Modelling, Cartesian Fourier-Transform, Spherical Fourier-Transform

I. INTRODUCTION

Knowledge of antenna radiation pattern is very important for radio channel modelling and estimation of parameters like direction-of-arrival (DoA). As stated in literature, the radiation pattern has to be known in angular domain, as well as in polarisation domain [1]. Furthermore, the antenna has to be known in frequency domain for e.g. broadband applications. Simple relying on sampled polarimetric beam patterns does not fit, if e.g. the antenna has to be known at arbitrary points. Therefore a model, describing the antenna continuously in each dimension, is necessary, which allows the calculation of the polarimetric antenna response at arbitrary points.

Methods to model frequency independent antennas are the EADF [2], the Spherical Harmonics (SH) [3], [4] or the Vector Spherical Harmonics (VSH) [5] approach. From literature, methods which incorporate also the frequency domain are fitting model based [6], VSH with Slepian decomposition [7] or Spherical Modes Expansion method with Singular Expansion method [8]. Here, we propose a straight forward extension of the EADF approach to incorporate also frequency dependence of the antenna (full 3D description), we call ETADF. We describe the ETADF in a compact notation form, using tensor algebra.

The rest of the paper is organized as follows: we introduce the basic antenna model and two ways of Fourier based antenna description in section II. Section III describes the ETADF, which incorporates also de-noising of measured antenna responses. An efficient method for antenna response interpolation from ETADF is stated in section IV. Model order estimation for ETADF is discussed in section V. Section VII concludes the paper.

Scalars, column vectors, matrices and tensors are notational distinguished as follows: Scalars are italic letters, vectors (in column format, unless declared otherwise) are bold faced letters, matrices are bold faced capitals, and tensors are bold faced upper-case calligraphic letters. We define the matrix operations $(\cdot)^T$, $(\cdot)^\dagger$ and $(\cdot)^H$ as the Transpose, pseudo-inverse and hermitian of a matrix, respectively. The Frobenius norm of a matrix is stated as $\|\cdot\|_F$. Real part and imaginary part of a complex number are depicted as $\Re\{\cdot\}$ and $\Im\{\cdot\}$, respectively.

We define the q-mode product between a tensor $\mathcal{B} \in \mathbb{C}^{M_1 \times \dots \times M_q \times \dots \times M_Q}$ and a matrix $\mathbf{A} \in \mathbb{C}^{P_q \times \dots \times M_q}$ as $\mathcal{B} \times_q \mathbf{A}$, which is obtained by multiplying the q-mode unfolding $\mathcal{U}_{(q)}\{\cdot\}$ (column-order in accordance with [9]) of the tensor from the left-hand side by the matrix and inverse unfolding: $\mathcal{U}_{(q)}^{-1}\{\mathbf{A} \cdot \mathcal{U}_{(q)}\{\mathcal{B}\}\} \in \mathbb{C}^{M_1 \times \dots \times P_q \times \dots \times M_Q}$. Concatenation of two tensors along dimension q is defined as \sqcup_q .

II. ANTENNA DESCRIPTION AND ALGEBRAIC MODELLING

We assume an antenna, placed in the origin of a spherical coordinate system Fig. 1, with elevation angle ϑ in the range from $[-\pi/2, \pi/2]$ and azimuth angle φ in the range of $[-\pi, \pi]$. Polarisation of an impinging wave is defined according to the φ - ϑ -plane, spanned by the spherical coordinate system basis vectors \mathbf{k}_φ and \mathbf{k}_ϑ in the impingement point.

Antennas are commonly described as a linear, time invariant systems [10]. A plane electromagnetic wave \mathbf{e} at distance r in the antenna's far field is given by:

$$\begin{aligned} \mathbf{e}(\varphi, \vartheta, f) &= \frac{e^{-j2\pi r \frac{f}{c}}}{r} [\mathbf{k}_\varphi \quad \mathbf{k}_\vartheta] \begin{bmatrix} b_\varphi(\varphi, \vartheta, f) \\ b_\vartheta(\varphi, \vartheta, f) \end{bmatrix} \\ &= \frac{e^{-j2\pi r \frac{f}{c}}}{r} \mathbf{K}_{\varphi, \vartheta} \mathbf{b}(\varphi, \vartheta, f) \end{aligned} \quad (1)$$

with the speed of light c . An antenna is fully described by its polarimetric radiation pattern $\mathbf{b}(\varphi, \vartheta, f)$. In practise, this pattern is only known at discrete sampling points in spherical coordinates, by e.g. measurements in an anechoic chamber or simulations. Therefore, an antenna model is necessary to derive sampling points outside of the sampling grid.

An algebraic antenna model can be obtained from wave field modelling, which imposes an orthonormal decomposition of

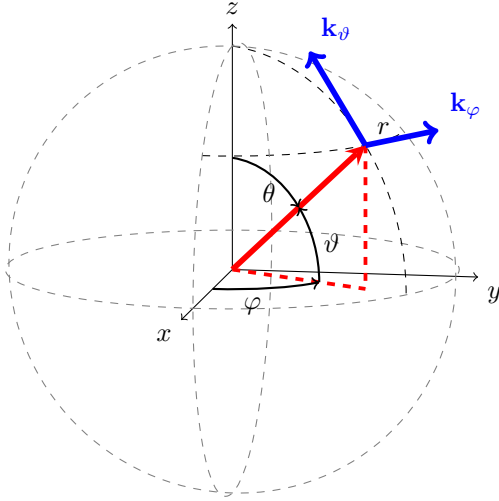


Figure 1. Spherical coordinate system and polarisation definition

the scalar antenna pattern [11]:

$$b_{\varphi|\vartheta}(\varphi, \vartheta, f) = \mathbf{g}^T \cdot \boldsymbol{\psi}(\varphi, \vartheta, f) \quad (2)$$

with $\boldsymbol{\psi}(\varphi, \vartheta, f)$ the basis functions of the decomposition and \mathbf{g} the antenna sampling vector. Note that the antenna sampling vector describes the antenna properties, whereas the basis function are independent of the antenna. Commonly Fourier basis functions are chosen, why wave field modelling becomes Fourier transformation. Two possible Fourier transformations are known from literature [12], which separates in the underlying coordinate system.

A. Cartesian Fourier Transformation

Cartesian Fourier Transformation (CFT) assumes equidistantly sampled data in a Cartesian coordinate system. The basis function $\boldsymbol{\psi}$ in 3D is given by:

$$\boldsymbol{\psi}_{\mu_x, \mu_y, \mu_z}^{CFT}(x, y, z) = e^{j2\pi\mu_x x} \cdot e^{j2\pi\mu_y y} \cdot e^{j2\pi\mu_z z} \quad (3)$$

As noticeable, the basis is given as product of the coefficient in each dimension and are therefore easily computable.

For application of the CFT to data measured in spherical coordinates, a projection of the angular domain on a plane is necessary. Several projections are known from map projections. Here, the Plate Carrée projection is used [13], because it preserves equidistant spacing, which is a key assumption to apply CFT. Based on the Plate Carrée projection, the relation between spherical coordinates and Cartesian coordinates is:

$$\begin{aligned} \varphi &\rightarrow x \\ \vartheta &\rightarrow y \\ f &\rightarrow z \end{aligned}$$

Because of the applied projection, distortions occur. Tissot's indicatrix [14] can be used to visualize distortions introduced by map projections. Small circles of equal radii are placed at several sphere locations, which is projected on the map

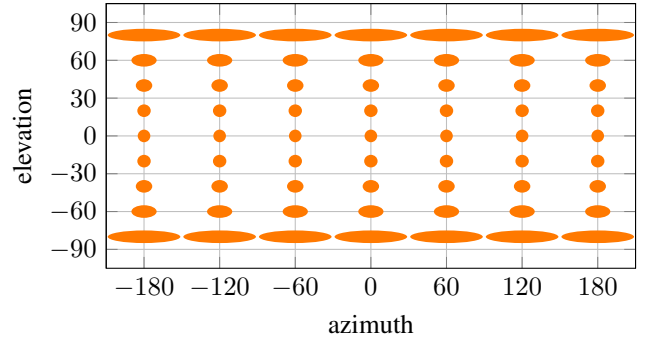


Figure 2. Tissot indicatrix for the Plate Carrée projection

afterwards. Modification of the circles in size and shape indicate, whether the projection is non-equal-area or non-conformal, respectively. The Tissot indicatrices for the Plate Carrée projection is shown in Fig. 2. Distortions do not occur for the longitudes but for the circles of latitude, because these circles are enlarged to the length of the equator. Therefore, the distortions increase to the poles. Accordingly, the main power contribution of the antenna should lie in the azimuth plane, because significant antenna energy at the poles would require more sampling points for proper modelling.

B. Spherical Fourier Transformation

Fourier transformation which considers spherical coordinates is the Spherical Fourier Transformation (SFT). The basis functions for the SFT in 3D are given by [15], where the radial part describes the frequency domain:

$$\boldsymbol{\psi}_{n,l,m}^{SFT}(r, \varphi, \vartheta) = \sqrt{\frac{1}{N_n^{(l)}}} \cdot j_l(k_{n,l}r) \cdot Y_{l,m}(\varphi, \vartheta) \quad (4)$$

with $j_l(k_{n,l}r)$ the spherical Bessel function of order l , $Y_{l,m}(\varphi, \vartheta)$ the spherical harmonic and $N_n^{(l)}, k_{n,l}$ defined according to [15].

Because the SFT basis functions are difficult to calculate, the interpolation is computationally cumbersome. Therefore, we skip the SFT approach.

III. EFFECTIVE TIME-APERTURE DISTRIBUTION FUNCTION (ETADF)

A. Antenna Fourier Transform

The polarimetric antenna radiation pattern is sampled according to the Nyquist criterion in azimuth steps $\Delta\varphi$, elevation steps $\Delta\vartheta$ and frequency steps Δf . The vectors of sampling points are give as:

$$\boldsymbol{\varphi} = [-\pi \dots \pi - \Delta\varphi]^T \in \mathbb{R}^{L_1 \times 1} \quad (5)$$

$$\boldsymbol{\vartheta} = [\pi/2 \dots -\pi/2]^T \in \mathbb{R}^{L_2 \times 1} \quad (6)$$

$$\mathbf{f} = 2\pi/B [-B/2 \dots B/2 - \Delta f]^T \in \mathbb{R}^{L_3 \times 1} \quad (7)$$

with B being the bandwidth. The sampled radiation pattern per polarisation k forms a tensor $\mathcal{B}_k(\boldsymbol{\varphi}, \boldsymbol{\vartheta}, \mathbf{f}) \in \mathbb{C}^{L_1 \times L_2 \times L_3}$. Because the polarisation components are orthogonal to each

other, we limit our investigations to a single polarisation in the following. Furthermore, we use co-elevation θ instead of elevation, which is given by transformation: $\theta = \pi/2 - \vartheta$ and therefore $\boldsymbol{\theta}' = [0 \dots \dots \pi]^T$.

The sampled radiation patterns are periodic in azimuth, why periodic extension of the elevation domain across the north pole is necessary [2]. The periodical radiation pattern is given by:

$$\begin{aligned} \mathcal{B}_k^{(p)}(\boldsymbol{\varphi}, \boldsymbol{\theta}, \mathbf{f}) &= -(\mathcal{B}_k(\boldsymbol{\varphi}', \boldsymbol{\theta}'', \mathbf{f}) \sqcup_1 \mathcal{B}_k(\boldsymbol{\varphi}'', \boldsymbol{\theta}', \mathbf{f})) \\ &\sqcup_2 \mathcal{B}_k(\boldsymbol{\varphi}, \boldsymbol{\theta}', \mathbf{f}) \in \mathbb{C}^{L_1 \times L_2 \times L_3} \quad (8) \\ \boldsymbol{\theta}'' &= [\pi - \Delta\theta \dots \Delta\theta]^T \\ \boldsymbol{\varphi}' &= [0 \dots \pi - \Delta\varphi]^T \\ \boldsymbol{\varphi}'' &= [-\pi \dots -\Delta\varphi]^T \end{aligned}$$

with $\boldsymbol{\theta} = [-\pi + \Delta\theta \dots \Delta\theta \dots \pi]^T$ the new sampling vector in co-elevation domain.

Utilising the periodic radiation pattern, the discrete Fourier transform (DFT) per dimension is given by:

$$\mathcal{G}_k = \mathcal{B}_k^{(p)}(\boldsymbol{\varphi}, \boldsymbol{\theta}, \mathbf{f}) \times_1 \mathbf{E}(\boldsymbol{\varphi}) \times_2 \mathbf{E}(\boldsymbol{\theta}) \times_3 \mathbf{E}(\mathbf{f}) \quad (9)$$

with the DFT matrices

$$\mathbf{E}(\boldsymbol{\varphi}) = \left(e^{j\boldsymbol{\varphi}\boldsymbol{\mu}_\varphi^T} \right)^\dagger \in \mathbb{C}^{L_1 \times L_1} \quad (10)$$

$$\mathbf{E}(\boldsymbol{\theta}) = \left(e^{j\boldsymbol{\theta}\boldsymbol{\mu}_\theta^T} \right)^\dagger \in \mathbb{C}^{L_2 \times L_2} \quad (11)$$

$$\mathbf{E}(\mathbf{f}) = \left(e^{j\mathbf{f}\boldsymbol{\mu}_f^T} \right)^\dagger \in \mathbb{C}^{L_3 \times L_3} \quad (12)$$

$$\boldsymbol{\mu}_\varphi = \left[-\frac{L_1}{2} \dots \frac{L_1}{2} - 1 \right]^T \in \mathbb{R}^{L_1 \times 1}$$

$$\boldsymbol{\mu}_\theta = \left[-\frac{L_2}{2} \dots \frac{L_2}{2} - 1 \right]^T \in \mathbb{R}^{L_2 \times 1}$$

$$\boldsymbol{\mu}_f = \left[-\frac{L_3}{2} \dots \frac{L_3}{2} - 1 \right]^T \in \mathbb{R}^{L_3 \times 1}$$

We state the tensor \mathcal{G}_k as the Time-Aperture Distribution Function (TADF) of the antenna for polarisation k .

B. Truncation and De-Noising

The Fourier transformed angular antenna pattern is concentrated in a limited area [2] and, because we assumed a time limited antenna impulse response, the same holds for the Fourier transformed frequency domain. Also, if the antenna pattern is oversampled, their Fourier transformation is band limited. Therefore, truncation of the TADF to energy carrying signal parts is possible, whereas other signal parts, which contain e.g. measurement noise, are negligible.

Truncation of the TADF has several advantages. First, the amount of data to store is reduced. Second, because noise carrying signal parts are dropped, the measured data are de-noised. Last, the computational complexity of the antenna interpolation (see next section) is reduced, because less data points have to be considered. Therefore, the truncated version of the TADF is called ETADF.

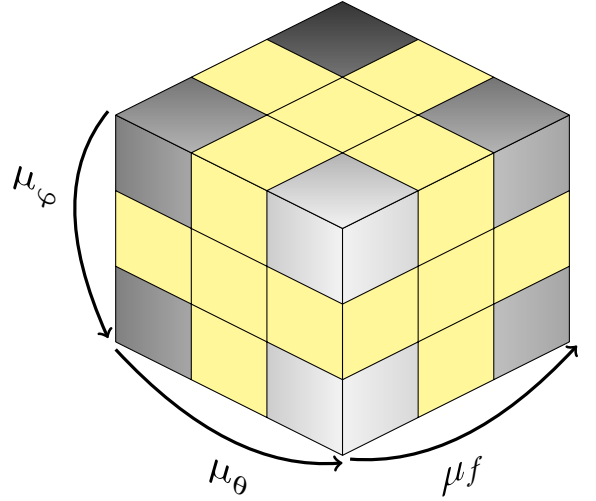


Figure 3. ETADF tensor $\bar{\mathcal{G}}_k$ with yellow sub-tensors where $\mu_\varphi = 0$, $\mu_\theta = 0$ or $\mu_f = 0$ holds

Calculation of the ETADF can be done by truncating the DFT matrices. The truncated DFT matrices are:

$$\bar{\mathbf{E}}(\boldsymbol{\varphi}) = \left(e^{j\boldsymbol{\varphi}\bar{\boldsymbol{\mu}}_\varphi^T} \right)^\dagger \in \mathbb{C}^{N_1 \times L_1} \quad (13)$$

$$\bar{\mathbf{E}}(\boldsymbol{\theta}) = \left(e^{j\boldsymbol{\theta}\bar{\boldsymbol{\mu}}_\theta^T} \right)^\dagger \in \mathbb{C}^{N_2 \times L_2} \quad (14)$$

$$\bar{\mathbf{E}}(\mathbf{f}) = \left(e^{j\mathbf{f}\bar{\boldsymbol{\mu}}_f^T} \right)^\dagger \in \mathbb{C}^{N_3 \times L_3} \quad (15)$$

$$\bar{\boldsymbol{\mu}}_\varphi = \left[-\frac{N_1-1}{2} \dots \frac{N_1-1}{2} \right]^T \in \mathbb{R}^{N_1 \times 1}$$

$$\bar{\boldsymbol{\mu}}_\theta = \left[-\frac{N_2-1}{2} \dots \frac{N_2-1}{2} \right]^T \in \mathbb{R}^{N_2 \times 1}$$

$$\bar{\boldsymbol{\mu}}_f = \left[-\frac{N_3-1}{2} \dots \frac{N_3-1}{2} \right]^T \in \mathbb{R}^{N_3 \times 1}$$

with N_1, N_2, N_3 are odd numbers and $N_1 < L_1$, $N_2 < L_2$, $N_3 < L_3$ for truncation. The ETADF for polarisation k is:

$$\bar{\mathcal{G}}_k = \mathcal{B}_k^{(p)}(\boldsymbol{\varphi}, \boldsymbol{\theta}, \mathbf{f}) \times_1 \bar{\mathbf{E}}(\boldsymbol{\varphi}) \times_2 \bar{\mathbf{E}}(\boldsymbol{\theta}) \times_3 \bar{\mathbf{E}}(\mathbf{f}) \quad (16)$$

An ETADF tensor is visualised in Fig. 3. The yellow fields refer to tensor entries, where $\mu_\varphi = 0$, $\mu_\theta = 0$ or $\mu_f = 0$ holds.

IV. EFFICIENT ANTENNA PATTERN INTERPOLATION

Based on the Fourier antenna model, calculation of the antenna radiation pattern for arbitrary azimuth, co-elevation and frequency is possible by inverse discrete Fourier transform (iDFT). The iDFT row-vectors are built according to the azimuth φ_0 , co-elevation θ_0 and frequency f_0 of interest:

$$\mathbf{d}(\varphi_0) = e^{j(\boldsymbol{\mu}_\varphi \varphi_0)} \in \mathbb{C}^{1 \times N_1} \quad (17)$$

$$\mathbf{d}(\theta_0) = e^{j(\boldsymbol{\mu}_\theta \theta_0)} \in \mathbb{C}^{1 \times N_2} \quad (18)$$

$$\mathbf{d}(f_0) = e^{j(\boldsymbol{\mu}_f f_0)} \in \mathbb{C}^{1 \times N_3} \quad (19)$$

$$\boldsymbol{\mu}_\varphi = \left[-\frac{N_1-1}{2} \dots \frac{N_1-1}{2} \right] \in \mathbb{R}^{1 \times N_1}$$

$$\boldsymbol{\mu}_\theta = \left[-\frac{N_2-1}{2} \dots \frac{N_2-1}{2} \right] \in \mathbb{R}^{1 \times N_2}$$

$$\boldsymbol{\mu}_f = \left[-\frac{N_3-1}{2} \dots \frac{N_3-1}{2} \right] \in \mathbb{R}^{1 \times N_3}$$

Applying the iDFT row-vectors to the ETADF tensor, the antenna radiation pattern for polarisation k is calculated as follows:

$$b_k(\varphi_0, \theta_0, f_0) = \bar{\mathcal{G}}_k \times_1 \mathbf{d}(\varphi_0) \times_2 \mathbf{d}(\theta_0) \times_3 \mathbf{d}(f_0) \quad (20)$$

Calculating the antenna pattern using the above formula needs $\mathcal{O}(4N_1N_2N_3)$ real-valued multiplications, which is computationally cumbersome if many points are requested. Therefore, methods for efficient calculation are necessary. In the following we present a two stage approach to 1) reduce the number of real-valued multiplications and 2) shrink the data dimension, which allows a much more efficient calculation.

A. Multiplication Reduction

The iDFT vectors feature a symmetry property, which is generally:

$$\mathbf{d} = \left[(\mathbf{\Pi} \cdot \mathbf{a})^H \quad 1 \quad \mathbf{a}^T \right]^T$$

$$\mathbf{a} = \left[e^{j\nu} \dots e^{j\frac{N-1}{2}\nu} \right]^T$$

with the permutation matrix $\mathbf{\Pi}$ as:

$$\mathbf{\Pi} = \begin{bmatrix} 0 & \dots & 1 \\ & \ddots & \\ 1 & \dots & 0 \end{bmatrix}$$

Due to this symmetry, the inner product of vector \mathbf{d} and an arbitrary vector $\mathbf{w} = [\mathbf{x}^T \quad y \quad \mathbf{z}^T]^T$ can be simplified as follows:

$$\mathbf{d}^T \cdot \mathbf{w} = \left[1 \quad \Re\{\mathbf{a}^T\} \quad \Im\{\mathbf{a}^T\} \right] \cdot \begin{bmatrix} y \\ \mathbf{z} + \mathbf{\Pi} \cdot \mathbf{x} \\ \mathbf{z} - \mathbf{\Pi} \cdot \mathbf{x} \end{bmatrix}$$

The number of real-valued multiplications is reduced by half. Vector \mathbf{w} is folded by either summation or subtraction of his left and right part.

This relationship is utilised to reduce the computational complexity of the iDFT. First, we define the folding matrix \mathbf{F} :

$$\mathbf{F}(N) = \begin{bmatrix} \mathbf{o}^T & 1 & \mathbf{o}^T \\ \mathbf{\Pi} & \mathbf{o} & \mathbf{I} \\ -j\mathbf{\Pi} & \mathbf{o} & j\mathbf{I} \end{bmatrix} \in \mathbb{R}^{N \times N} \quad (21)$$

$$\mathbf{I} \in \mathbb{R}^{\frac{N-1}{2} \times \frac{N-1}{2}}, \mathbf{o} \in \mathbb{R}^{\frac{N-1}{2} \times 1}, \mathbf{\Pi} \in \mathbb{R}^{\frac{N-1}{2} \times \frac{N-1}{2}}$$

with \mathbf{I} the identity matrix and \mathbf{o} vector of zero values. The ETADF folding is now given by:

$$\tilde{\mathcal{G}}_k = \bar{\mathcal{G}}_k \times_1 \mathbf{F}(N_1) \times_2 \mathbf{F}(N_2) \times_3 \mathbf{F}(N_3) \quad (22)$$

with $\tilde{\mathcal{G}}_k \in \mathbb{C}^{N_1 \times N_2 \times N_3}$ the folded ETADF. A folded ETADF tensor is depicted in Fig. 4, whereas the yellow blocks represent the sub-tensors where $\mu_\varphi = 0$, $\mu_\theta = 0$ or $\mu_f = 0$ holds.

The antenna radiation pattern for polarisation k can now be calculated by:

$$b_k(\varphi_0, \theta_0, f_0) = \tilde{\mathcal{G}}_k \times_1 \tilde{\mathbf{d}}(\varphi_0) \times_2 \tilde{\mathbf{d}}(\theta_0) \times_3 \tilde{\mathbf{d}}(f_0) \\ = \tilde{\mathcal{G}}_k \times_1 \tilde{\mathbf{d}}(\varphi_0) \times_2 \tilde{\mathbf{d}}(\theta_0) \times_3 \tilde{\mathbf{d}}(f_0) \quad (23)$$

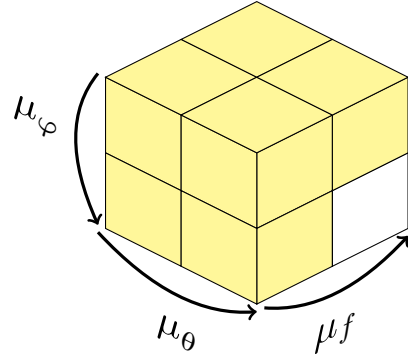


Figure 4. Folded ETADF tensor $\tilde{\mathcal{G}}_k$ with yellow sub-tensors where $\mu_\varphi = 0$, $\mu_\theta = 0$ or $\mu_f = 0$ holds

with the iDFT row-vectors:

$$\tilde{\mathbf{d}}(\varphi_0) = \left[1 \quad \Re\{e^{j\tilde{\mu}_\varphi \varphi_0}\} \quad \Im\{e^{j\tilde{\mu}_\varphi \varphi_0}\} \right] \in \mathbb{R}^{1 \times N_1} \quad (24)$$

$$\tilde{\mathbf{d}}(\theta_0) = \left[1 \quad \Re\{e^{j\tilde{\mu}_\theta \theta_0}\} \quad \Im\{e^{j\tilde{\mu}_\theta \theta_0}\} \right] \in \mathbb{R}^{1 \times N_2} \quad (25)$$

$$\tilde{\mathbf{d}}(f_0) = \left[1 \quad \Re\{e^{j\tilde{\mu}_f f_0}\} \quad \Im\{e^{j\tilde{\mu}_f f_0}\} \right] \in \mathbb{R}^{1 \times N_3} \quad (26)$$

$$\tilde{\mu}_\varphi = \left[1 \dots \frac{N_1-1}{2} \right] \in \mathbb{R}^{1 \times \frac{N_1-1}{2}}$$

$$\tilde{\mu}_\theta = \left[1 \dots \frac{N_2-1}{2} \right] \in \mathbb{R}^{1 \times \frac{N_2-1}{2}}$$

$$\tilde{\mu}_f = \left[1 \dots \frac{N_3-1}{2} \right] \in \mathbb{R}^{1 \times \frac{N_3-1}{2}}$$

The number of real-valued multiplications is reduced to $\mathcal{O}(2N_1N_2N_3)$.

B. Skipping Redundancy

Due to the periodical extension of the radiation pattern in elevation domain, redundant data are added in azimuth domain. This results in zero valued samples in the folded ETADF, which are ignorable during iDFT calculation.

First, matrices \mathbf{S}_e and \mathbf{S}_o are introduced, which selects even and odd rows of a matrix, respectively:

$$\mathbf{S}_e = \begin{bmatrix} 0 & 1 & 0 & 0 & \dots & 0 & 0 \\ 0 & 0 & 0 & 1 & \dots & 0 & 0 \\ & & & & \vdots & & \\ 0 & 0 & 0 & 0 & \dots & 1 & 0 \end{bmatrix} \in \mathbb{R}^{\frac{N_1-1}{2} \times N_1} \quad (27)$$

$$\mathbf{S}_o = \begin{bmatrix} 1 & 0 & 0 & 0 & \dots & 0 & 0 \\ 0 & 0 & 1 & 0 & \dots & 0 & 0 \\ & & & & \vdots & & \\ 0 & 0 & 0 & 0 & \dots & 0 & 1 \end{bmatrix} \in \mathbb{R}^{\frac{N_1+1}{2} \times N_1} \quad (28)$$

Second, matrices \mathbf{S}_r and \mathbf{S}_l are introduced, which selects the upper and lower rows of a matrix, respectively:

$$\mathbf{S}_u = \left[\mathbf{I}_{\frac{N_2+1}{2}} \quad \mathbf{O}_{\frac{N_2+1}{2}, \frac{N_2-1}{2}} \right] \in \mathbb{R}^{\frac{N_2+1}{2} \times N_2} \quad (29)$$

$$\mathbf{S}_l = \left[\mathbf{O}_{\frac{N_2-1}{2}, \frac{N_2+1}{2}} \quad \mathbf{I}_{\frac{N_2-1}{2}} \right] \in \mathbb{R}^{\frac{N_2-1}{2} \times N_2} \quad (30)$$

with $\mathbf{O}_{A,B} \in \mathbb{R}^{A \times B}$ matrix of all zeros and $\mathbf{I}_N \in \mathbb{R}^{N \times N}$ the identity matrix. For short hand notation, we abbreviate the

multiplication of the selection matrices with a folded ETADF:

$$\tilde{\mathbf{G}}_k^e = \tilde{\mathbf{G}}_k \times_1 \mathbf{S}_e \times_2 \mathbf{S}_u \quad (31)$$

$$\tilde{\mathbf{G}}_k^o = \tilde{\mathbf{G}}_k \times_1 \mathbf{S}_o \times_2 \mathbf{S}_l \quad (32)$$

and accordingly the multiplication with the iDFT row-vectors:

$$\tilde{\mathbf{d}}_e(\varphi_0) = \tilde{\mathbf{d}}(\varphi_0) \cdot \mathbf{S}_e^T \in \mathbb{R}^{1 \times \frac{N_1-1}{2}} \quad (33)$$

$$\tilde{\mathbf{d}}_o(\varphi_0) = \tilde{\mathbf{d}}(\varphi_0) \cdot \mathbf{S}_o^T \in \mathbb{R}^{1 \times \frac{N_1+1}{2}} \quad (34)$$

$$\tilde{\mathbf{d}}_u(\theta_0) = \tilde{\mathbf{d}}(\theta_0) \cdot \mathbf{S}_u^T \in \mathbb{R}^{1 \times \frac{N_2+1}{2}} \quad (35)$$

$$\tilde{\mathbf{d}}_l(\theta_0) = \tilde{\mathbf{d}}(\theta_0) \cdot \mathbf{S}_l^T \in \mathbb{R}^{1 \times \frac{N_2-1}{2}} \quad (36)$$

The antenna radiation pattern for polarisation k is now given by:

$$\begin{aligned} b_k(\varphi_0, \theta_0, f_0) &= \tilde{\mathbf{G}}_k \times_1 \mathbf{d}(\varphi_0) \times_2 \mathbf{d}(\theta_0) \times_3 \mathbf{d}(f_0) \\ &= \tilde{\mathbf{G}}_k^e \times_1 \tilde{\mathbf{d}}_e(\varphi_0) \times_2 \tilde{\mathbf{d}}_u(\theta_0) \times_3 \tilde{\mathbf{d}}(f_0) \\ &\quad + \tilde{\mathbf{G}}_k^o \times_1 \tilde{\mathbf{d}}_o(\varphi_0) \times_2 \tilde{\mathbf{d}}_l(\theta_0) \times_3 \tilde{\mathbf{d}}(f_0) \end{aligned} \quad (37)$$

Due to the skipped redundancy, the number of real-valued multiplications is $\mathcal{O}(N_1 N_2 N_3)$.

V. MODEL ORDER ESTIMATION

For truncation purpose, the number of significant signal parts have to be estimated in each ETADF dimension, which can be assumed as a model order estimation problem. As stated, we utilise an algebraic antenna model, why the unfolding of each dimension is generally modelled as:

$$\mathfrak{U}_{(q)} \left\{ \mathbf{B}_k^{(p)} \right\} = \mathbf{D}_{(q)} \cdot \mathfrak{U}_{(q)} \left\{ \mathbf{G}_k \right\} + \mathbf{N} \quad (38)$$

with $\mathbf{N} \sim \mathcal{N}(\mathbf{0}, \sigma_q^2 \mathbf{I})$ the matrix of circular, normal distributed noise; $\mathfrak{U}_{(q)} \left\{ \mathbf{G}_k \right\}$ the matrix of Fourier coefficients and $\mathbf{D}_{(q)}$ the DFT matrix. For notational convenience we introduce the following abbreviations:

$$\mathbf{B}_{k,(q)} = \mathfrak{U}_{(q)} \left\{ \mathbf{B}_k^{(p)} \right\} \in \mathbb{C}^{L_q \times \bar{L}_q}$$

$$\mathbf{G}_{k,(q)} = \mathfrak{U}_{(q)} \left\{ \mathbf{G}_k \right\} \in \mathbb{C}^{L_q \times \bar{L}_q}$$

wheras $\bar{L}_q = \prod_{i=1, i \neq q}^3 L_i$. Thus, equation (38) becomes:

$$\mathbf{B}_{k,(q)} = \mathbf{D}_{(q)} \cdot \mathbf{G}_{k,(q)} + \mathbf{N} \quad (39)$$

De-noising is achieved by band limiting the DFT matrix and therefore truncating parts of the Fourier coefficient matrix. We decompose model (39) into two parts, to account for P_q significant and $L_q - P_q$ truncated Fourier coefficients:

$$\begin{aligned} \mathbf{B}_{k,(q)} &= \sum_{l=1}^{P_q} \mathbf{D}_{(q)}(:, l) \cdot \mathbf{G}_{k,(q)}(l, :) \\ &\quad + \sum_{l=1+P_q}^{L_q} \mathbf{D}_{(q)}(:, l) \cdot \mathbf{G}_{k,(q)}(l, :) + \mathbf{N} \end{aligned} \quad (40)$$

wheras $\mathbf{D}_{(q)}(:, l)$ denotes the selection of the l -th column and $\mathbf{G}_{k,(q)}(l, :)$ the selection of the l -th row. Decomposition of model (39) is accomplished by considering the first P_q Fourier

coefficients, which are ordered descendingly according to their magnitude, and their corresponding DFT matrix vectors. In the following, P_q is denoted as model order. Estimation of model order P_q is conducted by statistical comparison of model order P_q and $P_q + 1$. Thus, the additional Fourier coefficients are tested, whether they significantly differ from zero, why the test's \mathcal{H}_0 hypothesis is: $\mathbf{G}_{k,(q)}(P_q + 1, :)^T = \mathbf{o}$.

A known statistical test here for is the F-test [16, p. 37], which test statistic for order P_q is:

$$F_{stat}(P_q) = \frac{\mathcal{L}(P_q) - \mathcal{L}(P_q + 1)}{\mathcal{L}(P_q + 1)} \cdot (L_q - P_q - 1) \quad (41)$$

The Fisher statistic is tested against the $1 - \alpha$ percentile point of the Fisher distribution, in order to verify the \mathcal{H}_0 hypothesis:

$$F_{stat}(P_q) < F_{1-\alpha}(2 \cdot \bar{L}_q, 2 \cdot \bar{L}_q \cdot (L_q - P_q - 1)) \quad (42)$$

with $\mathcal{L}(P_q)$ the sum of squared residuals according to model order P_q :

$$\mathcal{L}(P_q) = \left\| \mathbf{B}_{k,(q)} - \mathbf{D}_{(q)}^{(P_q)} \mathbf{D}_{(q)}^{(P_q)\dagger} \mathbf{B}_{k,(q)} \right\|_F^2 \quad (43)$$

Model orders from $P_q = 1 \dots L_q - 1$ are tested successively, until \mathcal{H}_0 hypothesis cannot be rejected based on a significance level α . If so, the additional Fourier coefficients, and also the following ones because of the magnitude ordering for model decomposition, are not significantly different from zero and can be truncated.

VI. SIMULATION

Verification of the ETADF approach based on HFSS simulation data of a horn antenna will be presented in the final paper.

VII. CONCLUSION

REFERENCES

- [1] M. Landmann, M. Kaske, and R. Thoma, "Impact of incomplete and inaccurate data models on high resolution parameter estimation in multidimensional channel sounding," *Antennas and Propagation, IEEE Transactions on*, vol. 60, no. 2, pp. 557–573, Feb 2012.
- [2] M. Landmann and G. Del Galdo, "Efficient antenna description for mimo channel modelling and estimation," in *Wireless Technology, 2004. 7th European Conference on*, Oct 2004, pp. 217–220.
- [3] G. Del Galdo, J. Lotze, M. Landmann, and M. Haardt, "Modelling and manipulation of polarimetric antenna beam patterns via spherical harmonics," in *Signal Processing Conference, 2006 14th European*, Sept 2006, pp. 1–5.
- [4] A. Schmitz, T. Karolski, and L. Kobbelt, "Using spherical harmonics for modeling antenna patterns," in *Radio and Wireless Symposium (RWS), 2012 IEEE*, Jan 2012, pp. 155–158.
- [5] C. Roblin, "Ultra compressed parametric modelling of uwb antenna measurements," in *Antennas and Propagation, 2006. EuCAP 2006. First European Conference on*, Nov 2006, pp. 1–8.
- [6] D. Werner and R. Allard, "The simultaneous interpolation of antenna radiation patterns in both the spatial and frequency domains using model-based parameter estimation," *Antennas and Propagation, IEEE Transactions on*, vol. 48, no. 3, pp. 383–392, Mar 2000.
- [7] W. Dullaert and H. Rogier, "Novel compact model for the radiation pattern of uwb antennas using vector spherical and slepian decomposition," *Antennas and Propagation, IEEE Transactions on*, vol. 58, no. 2, pp. 287–299, Feb 2010.
- [8] P. Koivisto, "Reduction of errors in antenna radiation patterns using optimally truncated spherical wave expansion," *Progress In Electromagnetics Research*, vol. 48, pp. 313–333, 2004.

- [9] L. D. Lathauwer, B. D. Moor, and J. Vandewalle, "A multilinear singular value decomposition," *SIAM J. Matrix Anal. Appl.*, vol. 21, pp. 1253–1278, 2000.
- [10] W. Wiesbeck, G. Adamiuk, and C. Sturm, "Basic properties and design principles of uwb antennas," *Proceedings of the IEEE*, vol. 97, no. 2, pp. 372–385, Feb 2009.
- [11] M. Doron and E. Doron, "Wavefield modeling and array processing, part i-spatial sampling," *Signal Processing, IEEE Transactions on*, vol. 42, no. 10, pp. 2549–2580, Oct 1994.
- [12] M. Costa, A. Richter, and V. Koivunen, "Unified array manifold decomposition based on spherical harmonics and 2-d fourier basis," *Signal Processing, IEEE Transactions on*, vol. 58, no. 9, pp. 4634–4645, Sep 2010.
- [13] J. P. Snyder and U. G. Survey, *Map projections—a working manual*. U.S. G.P.O. : For sale by the Supt. of Docs Washington, 1987.
- [14] D. M. Goldberg and J. R. G. III, "Flexion and skewness in map projections of the earth," *Cartographica*, vol. 42, no. 4, pp. 297–318, 2007.
- [15] Q. Wang, O. Ronneberger, and H. Burkhardt, "Rotational invariance based on fourier analysis in polar and spherical coordinates," *Pattern Analysis and Machine Intelligence, IEEE Transactions on*, vol. 31, no. 9, pp. 1715–1722, Sep 2009.
- [16] S. Haykin, Ed., *Adaptive Radar Signal Processing*. New York: Wiley-Interscience, 2007.